Pleistocene precession forcing of the upper ocean structure variations of the southern South China Sea*

TIAN Jun**, WANG Pinxian and CHENG Xinrong

(Laboratory of Marine Geology, Tongji University, Shanghai 200092, China)

Received March 1, 2004; revised March 25, 2004

Abstract The precession plays a dominant role in driving the tropical monsoon variations. Our high resolution, millennial scale marine isotope records from ODP Site 1143 in the southern South China Sea (SCS) present the detailed history of the upper ocean structure variations over the past 1.56 Ma on glacial/interglacial timescale. The cross spectral analyses between the Earth's orbital variations and the isotopic differences reveal a high coherency between the East-Asian-monsoon-related thermocline and nutricline variations of the SCS and the precession. The variations of monsoon-related isotopic difference between species also demonstrate periodicities of 11-, 12- and 14- thousand years near semi-precession which originates in the tropics, highlighting the importance of the precession in driving the east Asian monsoon changes.

Keywords: South China Sea, upper ocean structure, precession forcing.

The studies of the South Asian monsoon and African monsoon[1,2] indicate that the precession, as one of the astronomical forces of the Earth's climate changes, plays a dominant role in controlling the tropical climate changes. However, the Asian monsoon system consists of two subsystems, the South and East Asian monsoons. How does the east Asian monsoon respond to the astronomical forcing? The East Asian monsoons have influenced the upper ocean structure in the South China Sea (SCS)[3], such as the thermocline and nutricline changes, by driving the upwelling system. The late Pleistocene glacial/interglacial prevailing and declining of the East Asian winter and summer monsoons have directly led to the thermocline and nutricline variations in the northern and southern parts of the SCS[4]. Therefore, studies of the upper ocean structure can throw a light on revealing the relationship between the East Asian monsoon variations and the astronomical forcing. This paper will utilize the stable oxygen and carbon isotope records from ODP Site 1143 to discuss the Pleistocene upper ocean structure variations in the southern SCS, and further analyze its relationship with the astronomical forcing.

1 Samples and methods

1.1 Samples and age model

ODP Site 1143 (9°21.72′N, 113°17.11′E, at a water depth of 2772 m) lies in the Nansha area, with numerous coral reefs on the southern continental slope of the SCS, in an environment with great influence from the West Pacific Warm Pool (WPWP)[5] (Fig. 1). The upper 200 m at Site 1143 was triply cored using the advanced piston corer (APC) system. Samples were taken continuously at 10 cm apart in the 0~75.62 m interval from the three holes of Site 1143. Well-preserved specimens (clean, intact, with no signs of dissolution) of planktonic foraminifers *Globigerinoides ruber* (0.3~0.36 mm in diameter) and *Pulleniatina obliquiloculata* (0.3~0.4 mm in diameter), as well as benthic species, were chosen from each sample for stable oxygen and carbon isotope analyses. Sample preparation and stable isotope analyses were performed in the Laboratory of Marine Geology of Tongji University, Shanghai. Precision was regularly checked with a Chinese national carbonate standard (GBW04405) and the international standard NBS19; the standard deviation was 0.07‰ for $\delta^{18}O$ and 0.04‰ for $\delta^{13}C$ for the year 2000. Conversion to the international Pee Dee Belemnite (PDB) scale was performed using NBS19 and NBS18 standards. All

* Supported by the National Natural Science Foundation of China (Grant Nos. 40306011, 4999560 and 40321603) and the Major State Basic Research Development Program of China (Grant No. G2000078500)

** To whom correspondence should be addressed. E-mail: tianjun@mail.tongji.edu.cn

isotopic analytic details are given in Ref. [6].

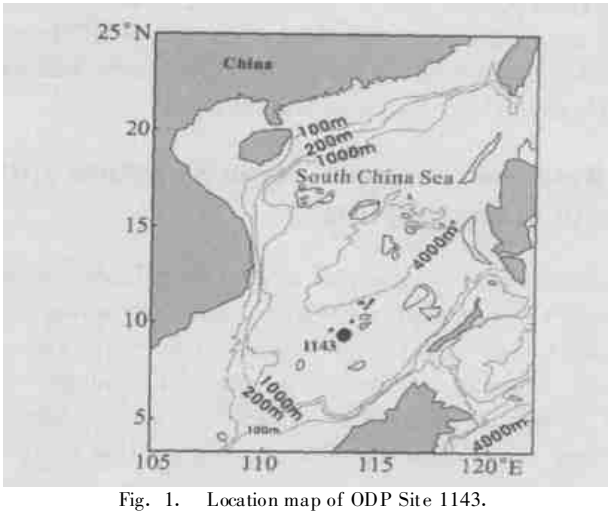

Fig. 1. Location map of ODP Site 1143.

The Plio-Pleistocene age model for Site 1143 was developed based on the benthic isotopic record, magnetostratigraphy and biostratigraphy[6]. By taking the benthic foraminifer $\delta^{18}O$ as the tuning material and the obliquity and precession as the tuning target, a 5 Ma astronomical timescale for Site 1143 was established using an automatic orbital tuning method. After the astronomical tuning, the depth of 190.77 m from Site 1143 corresponds to an age of about 5 Ma. The detailed method is given in Ref. [6].

1.2 Thermocline proxy

The vertical depth habitats of tropical planktonic foraminifers provide a primary tool for reconstructing surface water structure in paleo-oceans. Modern planktonic foraminiferal distribution indicates that shallow dwelling species such as *Globigerinoides ruber* and *G. sacculifer* dominate the assemblage when the surface mixed layer in an ocean is deep and the thermocline is depressed down to below the photic zone, and vice versa for the deeper thermocline dwelling species such as *P. obliquiloculata* and *Globorotalia tumida*[7~9]. In general, the subsurface water is cooler than that of the surface water. When thermocline shoals and the temperature gradient of the photic zone increases, the $\delta^{18}O$ difference between the surface and subsurface foraminifers increases; when thermocline deepens and the temperature gradient of the photic zone decreases, the $\delta^{18}O$ difference between the surface and subsurface foraminifers decreases[10~12]. The subsurface water enriches organic carbon but depletes $\delta^{13}C$, whereas this is reverse in the surface water. When nutricline shoals and the nutrient gradient increases, the $\delta^{13}C$ difference between the surface and subsurface foraminifers decreases and *vice versa*[10~13]. These kinds of researches had been successfully applied to the reconstruction of the east equatorial Pacific upper ocean structure variations in the late Pliocene and Pleistocene[10~13], and also applied to the open west Pacific for the past 2 Ma[14,15].

In this study, we used $\delta^{18}O$ and $\delta^{13}C$ difference between the thermocline species *P. obliquiloculata* and the mixed layer species *G. ruber*, hereinafter referred to as $\Delta\delta^{18}O$ (P-G) and $\Delta\delta^{13}C$ (P-G), as the thermocline and nutricline proxies respectively. In the open western equatorial Pacific and the SCS, *P. obliquiloculata* lives close to −150 m in the middle or the uppermost thermocline[16]. Modern *G. ruber* lives about 30 ~ 60 m in the upper mixed layer[17]. The variations of the $\delta^{18}O$ and $\delta^{13}C$ differences between these two species should well reflect the upper ocean structure changes.

2 Glacial/interglacial changes of the upper ocean structure

The time series of $\Delta\delta^{18}O$ (P-G), where the *G. ruber* $\delta^{18}O$ is subtracted from the *P. obliquiloculata* $\delta^{18}O$, is plotted in Fig. 2 against age after the 5-point running smoothing. The smoothing can minimize spikes that result from extremes in isotope values and from small differences in isotopic structures, especially at steep transitions from glacial stages to interglacial stages. In general, the peaks of the $\Delta\delta^{18}O$ (P-G) curve correspond to glacials, and the valleys to interglacials, indicating that the thermocline was shallow during interglacials but deep during glacials for the past 1.56 Ma. However, one exception exists that half of Marine Isotope Stage 11 (MIS 11) corresponds to the maximum of the $\Delta\delta^{18}O$ (P-G) but the other half to the minimum. Many geological records indicate that the MIS 11 was an abnormal period. For example, the amplitude of the precession components of the benthic $\delta^{18}O$ is much larger than that of the precession itself during MIS 11 when the global carbonate dissolution event, the so-called "Mid-Brunhes events", reached to its peak time[18]. Thus, the abnormal behavior of the thermocline variations of the SCS during MIS 11 is a local response to the global climate changes. The time series of $\Delta\delta^{13}C$ (P-G), where the *G. ruber* $\delta^{13}C$ is subtracted from the *P. obliquiloculata* $\delta^{13}C$, is plotted against age after the 5-point running smoothing, as seen in Fig. 3. Unlike the $\Delta\delta^{18}O$ (P-G), the $\Delta\delta^{13}C$ (P-G) does not

show the consistent glacial or interglacial variations. For example, in some interglacials such as MIS 9, 17, 21 and 23, the $\Delta\delta^{13}C$ (P-G) is high, indicating a deep nutricline depth, whereas in some other interglacials such as MIS 11, 15 and 19, the $\Delta\delta^{13}C$ (P-G) is shallow, indicating a shallow nutricline depth. These inconsistent interglacials $\Delta\delta^{13}C$ (P-G) variations also apply to the glacials, which implies that the factors influencing the nutricline variations are more complex than those influencing the thermocline variations in the southern SCS. Factors influencing thermocline changes in the SCS include sea surface temperature, the prevailing and declining of the monsoon as well as the upwelling. Because the SCS is the biggest marginal sea in the world, the terrestrial detritus contains ^{13}C-depleted but ^{12}C-enriched organic carbon from the adjacent chain islands and the main Asian continent. The quantity of these terrestrial detritus transported to the SCS through rivers will directly affect the nutrients and $\delta^{13}C$ values of the surface and subsurface waters, thus indirectly influencing the nutricline depth in the SCS.

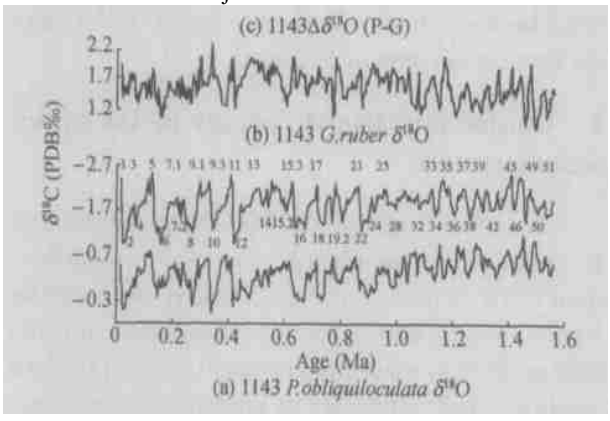

Fig. 2. Comparison of *P. obliquiloculata* $\delta^{18}O$ (a), *G. ruber* $\delta^{18}O$ (b) and $\delta^{18}O$(P-G) (c) after 5-point running smoothing in the last 1.56 Ma. The numbers denote some Marine Isotope Stages.

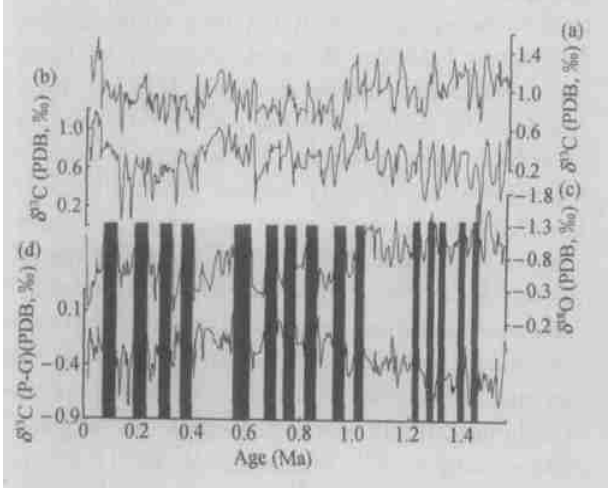

Fig. 3. Comparison of *G. ruber* $\delta^{13}C$ (a), *P. obliquiloculata* $\delta^{13}C$ (b), *P. obliquiloculata* $\delta^{18}O$ (c) and $\Delta\delta^{13}C$(P-G) (d) after 5-point running smoothing in the last 1.56 Ma. Shaded bars denote interglacials. Numbers denote some Marine Isotope Stages.

3 Response of upper ocean structure variations to orbital forcing

Cross spectral analysis is also an efficient way to measure the correlation between two time series at the frequency domain. Coherency and phase are two important parameters for cross spectral analysis. Coherency is a measure of the linear correlation between two time series over a given frequency when the phase difference is set to zero. Phase estimates over a specific frequency band indicate temporal (lead/lag) relationships between variables[20]. This method has been frequently used to study the climate response to the orbital and internal forcing, such as the case study of the physical mechanism of the Indian ocean monsoon[1]. This paper utilizes ETP (normalized sum of eccentricity, obliquity and negative precession) to represent the Earth's orbital forcing. The calculation of ETP follows the standard of Laskar[21].

Cross spectra analyses show that although the major Milankovitch cycles including 100 ka, 41 ka and 23 ka and 19 ka are remarkable in the spectrum of $\Delta\delta^{18}O$(P-G), the non-zero coherency exceeding 80% statistical level relative to the ETP only occurs at the 23 ka band (Fig. 4 (a)), which indicates a precession forcing of the temperature contrast of the upper ocean in the southern SCS. The seasonal reversing East Asian monsoon should have a great impact on the change of the upper ocean structure of the SCS, which results in the highlighted 23-ka cycle in the $\Delta\delta^{18}O$ (P-G) spectrum and the coherent relationship with the orbital forcing on the precession band. At Site 851 of the east equatorial Pacific, Ravelo and Shackleton[10] performed a cross spectral analysis of the $\delta^{18}O$ difference between *G. tumida* and *G. sacculifer* and between *G. tumida* and *N. dutertrei* and found that they are coherent only at the 19-ka band. Therefore, the thermocline variability they found at Site 851 is only in the precession band. The Indian ocean monsoon, an important component of the Asian monsoon system, shows a fairly strong spectral density on the precessional band with high coherency relative to the orbital forcing, as demonstrated by climatic proxy records such as pollen,

lithogenic grain size and opal flux[1, 22]. This spectral characteristic also holds true for the eolian dust records of Site 659, an indicator of the African monsoon[2]. Therefore, the 23-ka or 19-ka precessional cycles and their coherent relationships with the orbital forcing on the precession band are the characteristics of the monsoon system which is prevalent in tropical and low latitude regions.

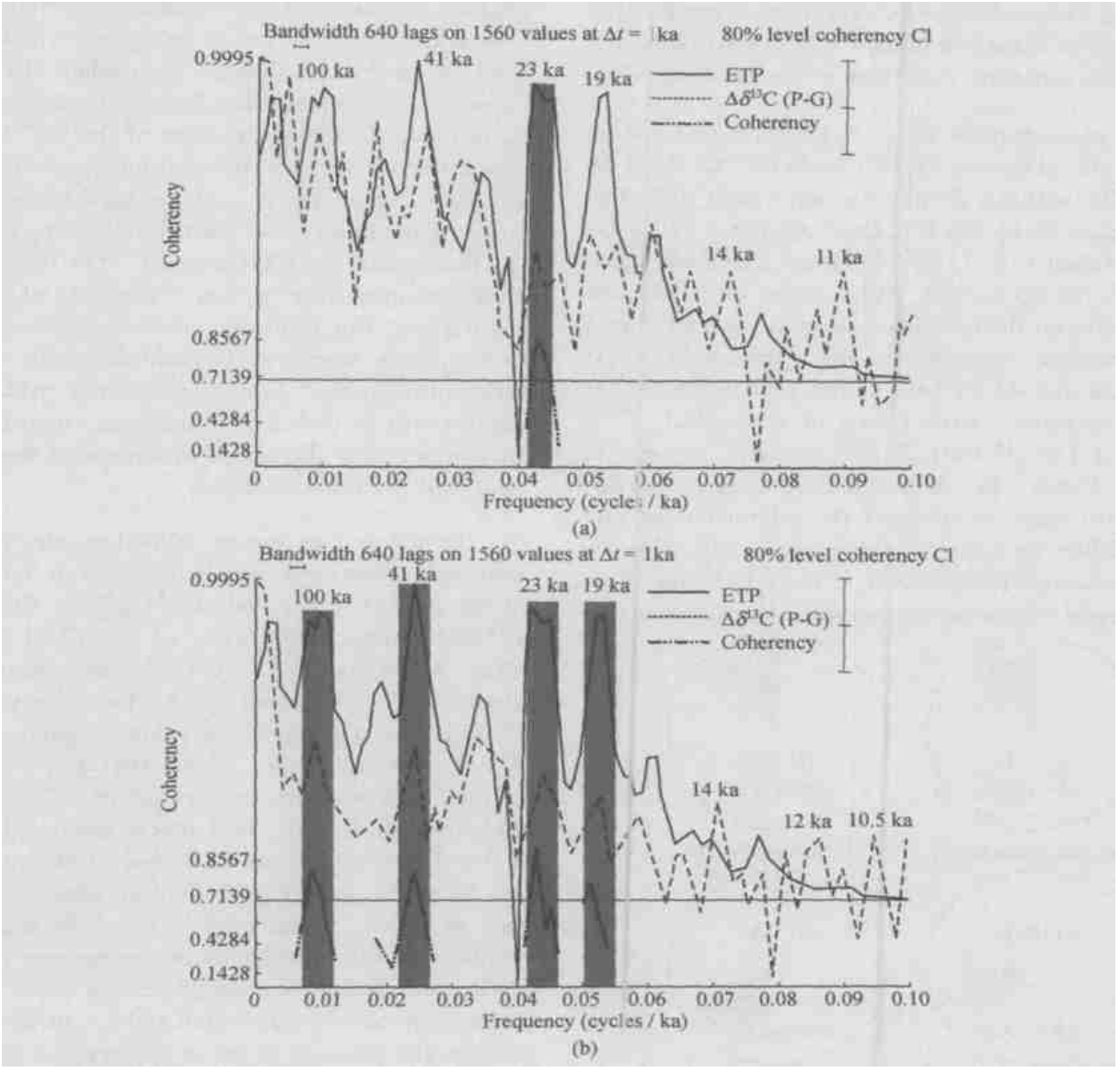

Fig. 4. Cross spectrum of ETP with $\Delta\,\delta^{18}O$(P-G) (a) and $\Delta\,\delta^{13}C$(P-G) (b), in the past 1.56 Ma. Solid lines denote the ETP spectrum; dashed lines the $\Delta\,\delta^{18}O$(P-G) or the $\Delta\,\delta^{13}C$(P-G) spectrum. Spectral densities are normalized and plotted on a log scale. The non-zero coherencies at 80% level are represented respectively by the horizontal solid lines. Grey areas denote the range of the Milankovitch periods of 100-ka, 41-ka, 23-ka and 19-ka. The analysis was performed using ARAND program.

Besides a high coherency with the orbital forcing at the 23-ka and 19-ka bands, the cross spectrum of the $\Delta\,\delta^{13}C$(P-G) with the ETP also reveals high coherencies at the obliquity (41 ka) and the eccentricity (100 ka) bands (Fig. 4(b)). However, the coherency at the precession bands are the highest among all, indicating a dominant control of the precession on the nutricline variations in the Pleistocene. Factors influencing $\delta^{13}C$ are more complex than those influencing $\delta^{18}O$. In addition to the east Asian monsoon variations, the terrestrial organic carbon discharge from the surrounding lands of the SCS and the production of the North Atlantic deep waters are also significant factors influencing the upper ocean nutrient contrast. The insolation at Northern Hemisphere at high latitudes determines the waxing and waning of the Northern Hemisphere ice sheet, and then further influences the erosion rate in the Asian internal conti-

nent, and necessarily influences the $\delta^{13}C$ difference of the upper ocean structure. The above factors could be ascribed to the interpretation of the coherent relationship of $\Delta\delta^{13}C$(P-G) with the ETP at all major Milankovitch cycles. However, one thing is certain that the precession plays a dominant role in controlling the upper ocean structure variations in the southern SCS.

The phase wheels (Fig. 5 (a) and (b)) show that the orbital forcing (ETP) leads $\Delta\delta^{18}O$(P-G) by $20.7^\circ \pm 20^\circ$ within a 23-a cycle, equivalent to 1.3 ka $\pm$1.27 ka, and by $21.4^\circ \pm 25.2^\circ$ within a 19-ka cycle, equivalent to 1.13 ka $\pm$1.33 ka. The small phases within the 23-ka and 19-ka cycles and the close phases between them indicate an precession forcing of the thermocline variations in the southern SCS. At the 100-ka and 41-ka bands, the ETP leads $\Delta\delta^{13}C$ (P-G) variations, with values of about $113.4^\circ \pm 23.5^\circ$ and $135.3^\circ \pm 21.7^\circ$ respectively, as seen in Fig. 5 (c) and (d). This indicates a coherent relationship between variations of the orbital forcing and the nutricline variations at these two bands. However, two negative phases occur at the 23-ka and 19-ka precession bands, with values of $-56.5^\circ \pm 16.8^\circ$ and $-78^\circ \pm 16.4^\circ$, respectively, as seen in Fig. 5 (e) and (f). The negative phases indicate that the orbital forcing lags behind the variations of the upper ocean nutrient contrast at the precession band by about 3.6 ~4.1 ka, which seems to be opposite to the traditional Milankovitch theory. To explain the negative phase relationships, other forcing mechanisms must be introduced to the variations of the $\Delta\delta^{13}C$(P-G). The influence of the introduced forcing should be bigger than that of the orbital forcing; subsequently it weakens the influence of the orbital forcing and makes the phase with the ETP negative. The forcing mechanism is supposed to happen in the tropical or equatorial regions. Due to its own characteristics, the global carbon cycle seems to be considered as the other mechanism beyond insolation forcing, which might explain why in the east[23] and west tropical Pacific, the variations of the $\Delta\delta^{13}C$ difference of the upper ocean lead the ETP variations.

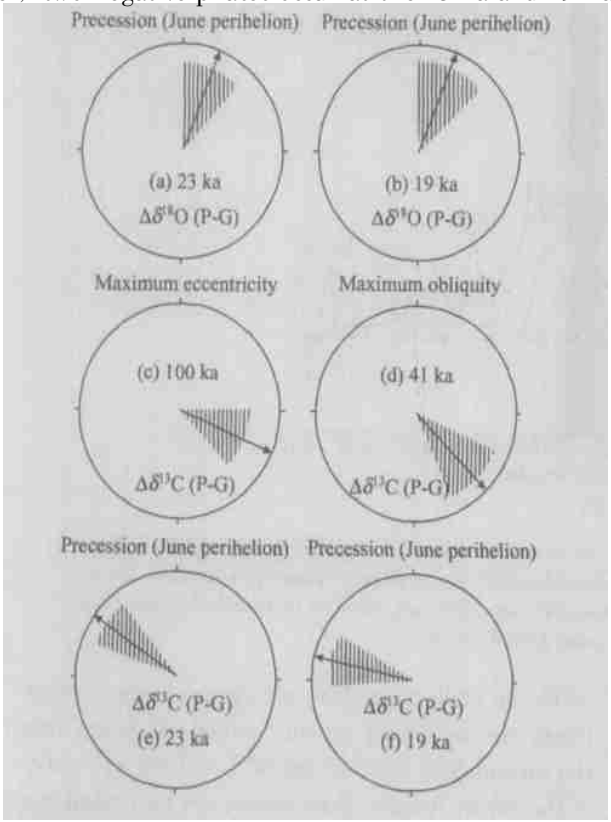

Fig. 5. Phase wheels of the $\Delta\delta^{18}O$(P-G) and the $\Delta\delta^{13}C$(P-G) relative to the ETP. (a) $\Delta\delta^{18}O$(P-G), at the 23-ka band; (b) $\Delta\delta^{18}O$(P-G), at the 19-ka band; (c) $\Delta\delta^{13}C$(P-G), at the 100-ka band; (d) $\Delta\delta^{13}C$(P-G), at the 41-ka band; (e) $\Delta\delta^{13}C$(P-G), at the 23-ka band; (f) $\Delta\delta^{13}C$(P-G), at the 19-ka band. The phase values are from Table 1.

In addition to regular Milankovitch cycles, the semi-precession cycles are highlighted in both spectra of the $\Delta\delta^{18}O$(P-G) and $\Delta\delta^{13}C$(P-G) for the past 1.56 Ma, such as 10.5 ka, 11 ka, 12 ka and 14 ka (Fig. 4 (a) and (b)). The semi-precession cycle is absent in the spectrum of the Earth's parameters (ETP), and the global ice volume changes (benthic $\delta^{18}O$), but highlighted in the spectra of the simulated maximum summer temperature at (0°N, 20°E)[24] and the dust flux of the tropical north Atlantic[25]. The pollen records from ODP Site 1144 in the northern SCS also show strong semi-precession cycles[26], such as 13 ka, 10 ka and 9 ka[26]. The alignment of perihelion with each equinox during one precession cycle can produce a semi-precession cycle which is phase-coupled with precession and eccentricity, analogous to the semi-annual cycle produced by the passage of the sun over the equator twice each year[25]. Some numerical models[27,28] require an approximately 10-ka free oscillation to produce much larger 100-ka response to weak eccentricity forcing. The model of Short et al.[24] demonstrated a strong linkage between low-latitude semi-precession and 100-ka cycles. The abundant semi-precession cycles in the isotopic differences of Site 1143 further highlight the importance of the tropics in the global climate changes.

4 Concluding remarks

This paper has reconstructed the thermocline and nutricline variations of the southern SCS for the past

1.56 Ma, based on $\delta^{18}O$ and $\delta^{13}C$ differences between the surface and subsurface planktonic foraminifers from ODP Site 1143. The thermocline was deep during glacials but shallow during interglacials. However, the nutricline does not follow this regulation but shows inconsistent variations during glacials or interglacials, which indicates that the factors influencing nutricline variations are far more complex than those influencing thermocline variations. Cross spectral analyses between the isotopic differences and the ETP demonstrate that precession is the dominant orbital force controlling the upper ocean structure variations in the southern SCS. Abundant semi-precession cycles have also been found in the $\Delta\delta^{18}O$(P-G) and $\Delta\delta^{13}C$(P-G) records. Because the upper ocean structure changes have been influenced by the East Asian monsoon to a great extent, we can infer that the precession plays a dominant role in modulating the East Asian monsoon variations. This forcing mechanism of the East Asian monsoon is analogous to those of the South Asian monsoon and African monsoon.

Acknowledgement The authors would like to thank the Ocean Drilling Program (ODP) for providing samples for this research.

References

1 Clemens, S. C. et al. Forcing mechanisms of the Indian Ocean monsoon. Nature, 1991, 353: 720.
2 Tiedemann, R. et al. Astronomic timescale for the Pliocene Atlantic $\delta^{18}O$ and dust flux records from Ocean Drilling Program Site 659. Paleoceanography, 1994, 9: 619.
3 Wang, L. et al. East Asian monsoon climate during the late Pleistocene: high-resolution sediment records from the South China Sea. Marine Geology, 1999, 156: 245.
4 Huang, B. et al. Foraminiferal responses to upwelling variations in the South China Sea over the last 220000 years. Mar. Micropaleontol., 2002, 47: 1.
5 Wang, P. et al. Proc. ODP Init. Reports 184. Ocean Drilling Program College Station, TX, 2000.
6 Tian, J. et al. Astronomically tuned Plio-Pleistocene benthic $\delta^{18}O$ records from South China Sea and Atlantic-Pacific comparison. Earth Planet Sci. Lett., 2002, 203: 1015.
7 Fairbanks, R. et al. Vertical distribution and isotopic fractionation of living planktonic foraminifera from the Panama Basin. Nature, 1982, 298: 841.
8 Thunell, R. et al. Seasonal variation in the flux of planktonic foraminifera: Time series trap results from the Panama Basin. Earth Planet Sci. Lett., 1983, 64: 44.
9 B$\acute{e}$, A. et al. Standing stock, vertical distribution and flux of planktonic foraminifera in the Panama Basin, Mar. Micropaleontol., 1985, 9: 307.
10 Ravelo, A. et al. Evidence for surface-water circulation changes at site 851 in the eastern tropical Pacific Ocean. Proc. ODP Sci. Results, 1995, 138: 503.
11 Cannariato, K. et al. Pliocene-Pleistocene evolution of eastern tropical Pacific surface water circulation and thermocline depth. Paleoceanography, 1997, 12: 805.
12 Chaisson, W. et al. Pliocene development of the east-west hydrographic gradient in the equatorial Pacific. Paleoceanography, 2000, 15: 497.
13 Farrell, J. et al. Upper ocean temperature and nutrient contrasts inferred from Pleistocene planktonic foraminifer $\delta^{18}O$ and $\delta^{13}C$ in the eastern equatorial Pacific. Proc. ODP Sci. Results, 1995, 138: 289.
14 Berger, W. et al. Quaternary oxygen isotope records of pelagic foraminifers: Site 806, Ontong Java Plateau. Proc. ODP Sci. Results, 1993, 130: 381.
15 Schmidt, H. et al. Quaternary carbon isotope record of pelagic foraminifers: Site 806, Ontong Java Plateau, Proc. ODP Sci. Results, 1993, 130: 397.
16 Schmidt, G. et al. Global calibration of ecological models for planktic foraminifera from coretop carbonate oxygen-18. Mar. Micropaleontol., 2002, 44: 125.
17 Hemleben, C. et al. Modern Planktonic Forminifera. New York: Springer-Verlag, 1989, 15~17.
18 Imbrie, J. et al. On the structure and origin of major glaciation cycles, 1, Linear responses to Milankovitch forcing. Paleoceanography, 1992, 7: 701.
19 Wang, P. et al. Carbon reservoir changes preceded major ice-sheets expansion at the mid-Brunhes event, Geology, 2002, 31: 239.
20 Ruddiman, W. et al. Earth's Climate: Past and Future. New York: W. H. Freeman and Company, 2000, 174~192.
21 Laskar, J. The chaotic motion of the solar system: A numerical estimate of the size of the chaotic zones. Icarus, 1990, 88: 266.
22 Prell, W. et al. Coherent response of Arabian Sea upwelling and pollen transport to Late Quaternary monsoonal winds. Nature, 1986, 323: 526.
23 Mix, A. et al. Benthic foraminifer stable isotope record from site 849 (0~5 Ma): local and global climate changes. Proc. ODP Sci. Results, 1995, 138: 371.
24 Short, D. et al. Filtering of Milankovitch cycles by Earth's geography. Quaternary Research, 1991, 35: 157.
25 Rutherford, S. et al. Early onset and tropical forcing of 100000-year Pleistocene glacial cycles. Nature, 2000, 408: 72.
26 Sun, X. et al. Deep-Sea Pollen Record over the Last Million Years from the South China Sea and East Asian Monsoon. Marine Geology, 2003, 201: 97.
27 Maasch, K. et al. Low-order dynamical model of global climatic variability over the full Pleistocene. J. Geophys. Res., 1990, 95: 1955.
28 Saltzman, B. et al. Late Pleistocene climate trajectory in the phase space of global ice, ocean state, and CO_2: Observations and theory. Paleoceanography, 1994, 9: 767.